Benzene ring orientation in uniaxial-planar poly(ethylene terephthalate) films

P. Lapersonne*, D. I. Bower and I. M. Ward†
IRC in Polymer Science and Technology, University of Leeds, Leeds LS2 9JT, UK
(Received 26 September 1990; accepted 21 January 1991)

A study is presented of the benzene ring orientation in a series of eight films of poly(ethylene terephthalate) drawn at constant width under constant force above the glass transition temperature. For each sample, seven orientation moment averages, P^r_{lmn}, for the overall benzene ring distribution were determined from a combination of Raman and infrared spectroscopic measurements. Comparison of orientation moment averages calculated with and without the assumption of a uniaxial Raman tensor, and with and without a refractive index correction to the Raman intensities, leads to the conclusion that the seven P^r_{lmn} are given, to a good approximation, by the simplest calculation assuming a uniaxial Raman tensor and neglecting the refractive index correction. The seven P^r_{lmn} were used to calculate the 'most probable' distribution function and the isometric projections of this distribution have been produced. The results indicate that the C_1–C_4 axis shows an approximately uniaxial overall distribution with a slight tendency to be more oriented out of the plane of the film and that the benzene rings tend to lie in the plane of the film. From a combination of these results with those of earlier X-ray measurements, the amorphous and crystalline contributions to the overall molecular orientation were obtained. The results show that the benzene ring planes are preferentially oriented towards the plane of the film only in the crystalline phase and have an almost uniaxial distribution around the draw direction in the amorphous phase. It has been shown that, in the amorphous phase as well as in the crystalline phase, the benzene rings tend to lie in the plane defined by the draw direction and the C_1–C_4 axis.

(Keywords: benzene ring; orientation; films; polyethylene terephthalate)

INTRODUCTION

The first drawing step in the commercial production of poly(ethylene terephthalate) (PET) films involves stretching an isotropic quenched film between moving rollers and has three main characteristics: it is a uniaxial-planar deformation (at constant width); drawing occurs at constant force; the draw temperature is close to or above the glass transition temperature[1].

A study of the kinetics[1] of a laboratory drawing procedure which simulates this step, and initial measurements on the structures produced[2] have already been published. This procedure involves drawing wide films under a constant dead load. The crystalline orientation and morphology[3], and the benzene ring normal orientation[4] have been described for films drawn under different conditions of load and temperature. More information, especially about the chain axis orientation and a complete description of the benzene ring orientation, is required for further understanding of this type of stretching. A combination of two convenient spectroscopic methods can be applied to obtain information about the benzene ring orientation: Raman scattering and infrared absorption. The thickness of the films ranges from 30 to 50 μm, which is ideal for infrared spectroscopy at 875 cm^{-1} and for Raman spectroscopy at 1616 cm^{-1}.

The combination of these two spectroscopic measurements has been applied to eight of the films previously studied, which were drawn at 90°C and 100°C. Because the films are biaxially oriented, normal-film and tilted-film infrared experiments have to be carried out and Raman intensities have to be measured with the polarizer and analyser directions parallel to the three principal directions of the films. In earlier work[5], where it was assumed that the 1616 cm^{-1} Raman line tensor was uniaxial, it was shown that this combination of measurements allows the determination of seven quantities P^r_{lmn}, which are orientation moment averages of the distribution function of the benzene ring. Those averages include the four second-order moment averages P^r_{2mn} and three of the nine fourth-order moment averages P^r_{4mn}. It has been shown in a recent paper[6] that the Raman tensor for the 1614 cm^{-1} line of a model compound for PET is not uniaxial. The theory of the study of orientation by infrared absorption and Raman scattering will therefore be discussed for biaxially oriented films without the assumption of a uniaxial Raman tensor. The seven moment averages P^r_{lmn}, calculated with and without this assumption, will be compared for two of the films studied.

The seven measured values P^r_{lmn} on the eight films have been used to estimate the orientation distribution function for the benzene rings by the calculation of the most probable distribution function $N_{mp}(\theta, \phi, \psi)$ introduced by Bower[7]. Stereographic projections of this distribution function for the C_1–C_4 axis and the plane normal of the benzene ring will be produced.

* Present address: Rhône-Poulenc Recherches, Centre de Recherches des Carrières, 85 ave des Frères-Perret, BP 62-69192, Saint-Fons Cedex, France
† To whom correspondence should be addressed

0032-3861/92/061266-11

From earlier work[3] dealing with the crystalline phase of these samples, the four second-moment averages for the crystalline phase P^r_{2mn}(crystal) can be calculated. The four P^r_{2mn}(amorphous) characterizing the amorphous phase can then also be deduced.

Infrared measurements using polarized radiation can also be used to obtain information about the relationship between conformational changes and the development of orientation. This is discussed in the accompanying paper[8].

THEORY

Reference axes and orientation moment averages

$OX_1X_2X_3$ is the system of orthogonal axes attached to the sample. OX_3 is parallel to the draw direction (i.e. the machine direction, MD) and OX_1 lies in the plane of the film and is parallel to the transverse direction (TD). In this set of axes, the deformation tensor of the films is:

$$\begin{bmatrix} 1 & 0 & 0 \\ 0 & 1/\lambda & 0 \\ 0 & 0 & \lambda \end{bmatrix}$$

where λ is the draw ratio in the draw direction (i.e. MD). It should be noted that this system of macroscopic reference axes is different from that used in the earlier work on these samples[3,4]. The two systems are related by a simple circular permutation.

$Ox^r_1x^r_2x^r_3$ are the axes fixed in the benzene ring. The definition of this set of axes is the same as that used by Jarvis and co-workers[5,9]. As shown in *Figure 1*, Ox^r_3 is parallel to the direction C_7–C_8 and Ox^r_1 lies in the plane of the benzene ring: this plane is defined by C_2, C_3, C_5 and C_6.

The orientation of the unit defined by $Ox^r_1x^r_2x^r_3$ with respect to the macroscopic set of axes $OX_1X_2X_3$ can be described by the three Euler angles θ^r, ϕ^r and ψ^r, as defined in ref. 5. It is then possible to introduce the P^r_{lmn}, the orientation moment averages of this particular distribution, as:

$$P^r_{lmn} = \langle p_{lmn}(\theta^r, \phi^r, \psi^r) \rangle$$

where the angle brackets denote an average over the structural units of the sample. The functions p_{lmn}, which are generalized spherical harmonics, are given explicitly in ref. 5.

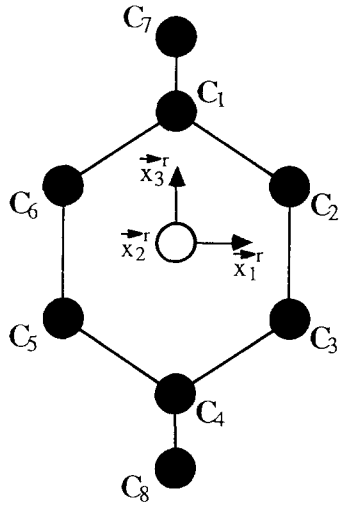

Figure 1 Ring axes $Ox^r_1x^r_2x^r_3$

Raman scattering

The study of Raman scattered intensities has already been developed to determine some of the benzene ring orientation moment averages P^r_{lmn} with $l = 2$ or 4 for uniaxially[10,11] and biaxially[5,9,12] oriented PET samples, assuming that the Raman tensor for the 1616 cm^{-1} line was uniaxial. It has been shown recently, however, that this assumption may not be quite correct[6]. A brief summary of the results of the calculations previously made by Bower[13,14] on the relationship between the Raman scattered intensities and the P^r_{lmn} is given here for biaxial orientation without any special assumption about the ratios of the principal components of the Raman tensor.

For any Raman line, the scattering intensity I_{ij}, with the polarization directions of the incident light and analyser parallel to the axes OX_i and OX_j respectively, is related to the orientation moment averages P_{lmn} for the principal axes of the corresponding Raman tensor by:

$$I_{ij} = N_0 I_0 \sum_{lmn} P_{lmn} A^{ij}_{lmn} \qquad (1)$$

where N_0 is the number of effective scatterers, I_0 is a constant depending on the incident light intensity and instrumental factors and A^{ij}_{lmn} are the second order functions of the three principal components of the Raman tensor $\alpha_1, \alpha_2, \alpha_3$ introduced by Jarvis *et al.*[5]. The influence of the refractive indices is neglected as in the earlier studies[5,9] but will be considered later.

The 1616 cm^{-1} Raman line for PET is due to an almost pure benzene ring vibration and its principal axes coincide with $Ox^r_1x^r_2x^r_3$. Therefore, for this line, the orientation moment averages involved in equation (1) are the P^r_{lmn}. It can be shown from ref. 12 that:

$$\begin{aligned} I'_{11} = {} & A + B(P^r_{200} - 6P^r_{220}) - 4F(P^r_{202} - P^r_{222}) \\ & + C(3P^r_{400} - 60P^r_{420} + 70P^r_{440}) \\ & - 2G(9P^r_{402} - 2P^r_{422} + 28P^r_{442}) \\ & + 4H(3P^r_{404} - 4P^r_{424} + P^r_{444}) \end{aligned} \qquad (2a)$$

$$\begin{aligned} I'_{22} = {} & A + B(P^r_{200} + 6P^r_{220}) - 4F(P^r_{202} + P^r_{222}) \\ & + C(3P^r_{400} + 60P^r_{420} + 70P^r_{440}) \\ & - 2G(9P^r_{402} + 2P^r_{422} + 28P^r_{442}) \\ & + 4H(3P^r_{404} + 4P^r_{424} + P^r_{444}) \end{aligned} \qquad (2b)$$

$$\begin{aligned} I'_{33} = {} & A - 2BP^r_{200} + 8FP^r_{202} + 8CP^r_{400} \\ & - 48GP^r_{402} + 32HP^r_{404} \end{aligned} \qquad (2c)$$

$$\begin{aligned} I'_{12} = {} & D + 2EP^r_{200} - 8GP^r_{202} + C(P^r_{400} - 70P^r_{440}) \\ & - (6GP^r_{402} - 56P^r_{442}) + 4H(P^r_{404} - P^r_{444}) \end{aligned} \qquad (2d)$$

$$\begin{aligned} I'_{13} = {} & D - E(P^r_{200} + 6P^r_{220}) + 4G(P^r_{202} + P^r_{222}) \\ & - 4C(P^r_{400} - 15P^r_{440}) + 4G(6P^r_{402} - P^r_{422}) \\ & - 16H(P^r_{404} - P^r_{424}) \end{aligned} \qquad (2e)$$

$$\begin{aligned} I'_{23} = {} & D - E(P^r_{200} - 6P^r_{220}) + 4G(P^r_{202} - P^r_{222}) \\ & - 4C(P^r_{400} + 15P^r_{440}) + 4G(6P^r_{402} + P^r_{422}) \\ & - 16H(P^r_{404} + P^r_{424}) \end{aligned} \qquad (2f)$$

where

$$A = \tfrac{1}{15}[3(1 + r_1^2 + r_2^2) + 2(r_1 + r_1 r_2 + r_2)]$$
$$B = \tfrac{1}{21}[3r_1^2 + 3r_2^2 - 6 + 2r_1 r_2 - r_1 - r_2]$$
$$C = \tfrac{1}{280}[3r_1^2 + 3r_2^2 + 8 + 2r_1 r_2 - 8r_1 - 8r_2]$$
$$D = \tfrac{1}{15}[r_1^2 + r_2^2 + 1 - (r_1 r_2 + r_1 + r_2)]$$
$$E = \tfrac{1}{42}[r_1^2 + r_2^2 - 2 - 2(2r_1 r_2 - r_1 - r_2)]$$
$$F = \tfrac{1}{14}(r_1 - r_2)(3r_1 + 3r_2 + 1)$$
$$G = \tfrac{1}{112}(r_1 - r_2)(r_1 + r_2 - 2)$$
$$H = \tfrac{7}{72}(r_1 - r_2)^2$$

and

$$I'_{ij} = \frac{I_{ij}}{\alpha_3^2 I_0 N_0}$$

with $r_1 = \alpha_1/\alpha_3$ and $r_2 = \alpha_2/\alpha_3$.

If the values of r_1 and r_2 are known, equations (2a) to (2f) are six simultaneous equations in the 14 quantities $(\alpha_3^2 I_0 N_0)^{-1}$, P^r_{lmn} for $l = 2$ and 4. If the Raman tensor is assumed to be uniaxial, then:

$$r_1 = r_2$$

and

$$F = G = H = 0$$

and the system of six equations used by Jarvis *et al.*[5,9] is obtained.

Infrared absorption

The relationships between the second-moment orientation and infrared absorbances for biaxially drawn films have already been developed by Jarvis *et al.*[5] and Cunningham *et al.*[15,16]. In the present study, only one absorption peak associated with a benzene ring vibration is considered, the 875 cm^{-1} peak. Its vibrational transition moment vector is normal to the plane of the benzene ring[16,17] ($\theta_m = 90°$).

For normal-film experiments, where the incident light is perpendicular to the plane of the film and the polarization direction is parallel to OX_3 or OX_1, the relationship between the experimentally observed absorbance A_i in the direction OX_i ($i = 1, 3$), is given by:

$$A_i = 0.4343\left\{4\pi k_i \frac{y_0}{\lambda} + \frac{2k_i^2}{(n_i + n_0)^2}\right\} \qquad (3)$$

where k_i, n_i are the imaginary and real parts of the complex principal refractive index for the electric vector in the direction OX_i, y_0 is the thickness of the film, λ is the infrared wavelength and n_0 is the refractive index of the medium surrounding the sample. For low values of k_i (<0.1), as in this work, the second term of this expression can be neglected. Thus k_1 and k_3 can be determined easily.

For tilted-film experiments, when the plane wave is incident at an angle of θ_i on the plane face and when the electric vector lies in the plane of incidence that coincides with OX_2X_i ($i = 1, 3$), it can be shown for low k_i that the absorbance $A_{2i}(\theta_i)$ is given by:

$$A_{2i}(\theta_i) = 0.4343 \frac{4\pi y_0}{\lambda} \frac{n_i}{n_2} \frac{n_2^2 \kappa_i + n_0^2 \sin^2\theta_i (\kappa_2 - \kappa_i)}{(n_2^2 - n_0^2 \sin^2\theta_i)^{1/2}} \qquad (4)$$

with $\kappa_i = k_i/n_i$. Two values of k_2 can be calculated for $i = 1$ and $i = 3$.

As in previous work, the three principal refractive indices used in these equations are the optical refractive indices obtained by measurements with an Abbe refractometer.

From these values of k_i and n_i, it is possible to calculate quantities $\bar{\phi}_i$ proportional to the imaginary part of the average complex principal polarizability. These quantities are related to the orientation moment averages P^r_{lmn} as follows. The quantity $\phi_i = \frac{4}{3}\pi N \langle \alpha''_i \rangle$, where N is the concentration of absorbing species per unit volume and $\langle \alpha''_i \rangle$ is the imaginary part of the average complex principal polarizability, is given for small absorbances to a good approximation by:

$$\phi_i = \frac{6 n_i k_i}{(n_i^2 + 2)^2} \qquad (5)$$

For a Lorentzian absorption peak, the integrated intensity is given by:

$$\bar{\phi}_i = \int_{-\infty}^{+\infty} \phi_i(\lambda)\, d\lambda = \frac{\pi}{2} \phi_i^{peak} \Delta x_{1/2} \qquad (6)$$

with ϕ_i^{peak} the maximum value of ϕ_i for a peak of half-band width $\Delta x_{1/2}$. For an angle $\theta_m = 90°$, it can then be shown[5] that:

$$\frac{2\bar{\phi}_3 - \bar{\phi}_2 - \bar{\phi}_1}{\bar{\phi}_1 + \bar{\phi}_2 + \bar{\phi}_3} = -(P^r_{200} + 6P^r_{202}) \qquad (7a)$$

and

$$\frac{\bar{\phi}_1 - \bar{\phi}_2}{\bar{\phi}_1 + \bar{\phi}_2 + \bar{\phi}_3} = -2(P^r_{220} + P^r_{222}) \qquad (7b)$$

As the absorption region near 875 cm^{-1} is a summation of two Lorentzian peaks, at 872 cm^{-1} and 877 cm^{-1}, the quantities ϕ_i in these equations have been replaced by the sum over the two contributions.

Calculation of the crystallinity

The density of the film can be obtained from the average refractive index $\bar{n} = (n_1 + n_2 + n_3)/3$, using the following expression derived for PET films[18]:

$$d = 4.047 \frac{\bar{n}^2 - 1}{\bar{n}^2 + 2} \qquad (8)$$

Assuming a two phase model, the crystallinity χ_c is given by:

$$\chi_c = \frac{d - d_a}{d_c - d_a} \qquad (9)$$

where d_a is the amorphous density and d_c is the crystalline density. The value of d_a was assumed to be 1.335 for all samples. The value of the crystalline density for PET has been the subject of many studies[19–23] and has been proved to be dependent on the drawing process. It can, however, be concluded that this value must be fairly constant for the stretching conditions used in the present work and that d_c must be between 1.455 and 1.484, the extreme values for stretching with a drawing temperature around 100°C. Both extreme values will be considered in this study.

EXPERIMENTAL

Films

The preparation of the samples has been described in detail in an earlier paper[3]. Rectangular samples (10 mm long, 120 mm wide and 0.16 mm thick) were stretched under constant engineering stress simply by hanging a load on the sample. The central portion of these samples is characterized by a constant width. The kinematics of this type of stretching have been accurately described earlier[1]: first the deformation increases rapidly with time and then reaches an equilibrium plateau value characterized by the plateau draw ratio $\lambda_p(\sigma_0, T)$, which depends on stress and temperature. In this study only eight of the 26 films stretched under different conditions of load and temperature used in the previous work[3,4] will be analysed. These are four films stretched at constant width with a drawing temperature $T = 90°C$ and engineering stresses $\sigma_0 = 1.84$, 3.07, 4.30 and 5.52 MPa, and four films with $T = 100°C$ and $\sigma_0 = 1.23$, 2.46, 3.69 and 4.92 MPa. They were 'drawn with a short plateau'[1]: the state of orientation was frozen just after the equilibrium deformation was reached.

Raman measurements

The apparatus to record the Raman spectra has been described previously[24]. The 488 nm line of an argon ion laser is used to excite the spectra and a Coderg PHO double monochromator is used to analyse the spectra.

The experimental procedure used in this work differs slightly from the procedure described by Jarvis *et al.*[5,9]. In this study, only six of the nine possible scattering configurations will be considered. They correspond to the configurations X_1X_1, X_1X_3, X_2X_2, X_2X_3, X_3X_1 and X_3X_2, where X_iX_j represents a scattering configuration with the incident light parallel to OX_i and the Raman scattered light detected in direction OX_j. For each configuration, there are four combinations of polarization direction for the polarizer and the analyser. That gives 24 scattered intensities for one sample. For a given configuration and polarization direction of the polarizer, two intensities are measured for the two possible polarization directions of the analyser. A similar mathematical procedure to that used by Jarvis *et al.*[5] was used to scale these 12 sets of two intensity measurements for each sample to the same value of N_0I_0 with the largest intensity, I_{33}, equal to 100. As in the previous studies[5,9], there is good agreement between I_{ij} and I_{ji}, and the root mean square deviation for each calculated intensity is always smaller than 5 and usually smaller than 1.5.

Infrared measurements

The infrared spectra were recorded on a Perkin–Elmer 580B ratio recording spectrometer. Each sample was sandwiched with layers of nujol between two potassium bromide plates for normal-film experiments and between potassium bromide prisms for tilted-film experiments, so that $\theta_i = 45°$ and $n_0 = n_{KBr}$ = potassium bromide refractive index in equations (3) and (4). The value of k_2 used in the calculation of orientation moment averages is the mean of the two values obtained for the two tilted-film spectra (from $A_{21}(45°)$ and $A_{23}(45°)$). The normal-film and tilted-film experimental procedure of spectra recording and computer reconstruction has been previously described[5]. The minimum number of Lorentzian peaks was used to obtain a good fit to the spectrum between 700 and 1100 cm^{-1}. Position and half-intensity width were allowed to vary freely for the study of the first sample but were kept fixed afterwards for all the other samples. Good fits for the spectra of all films were obtained with this method.

For the study of the benzene ring orientation, two regions of the spectrum are of great interest. The region near 1017 cm^{-1}, giving information about the C_1–C_4 axis orientation, is unfortunately saturated for the normal-film spectra with the polarization direction parallel to the draw direction OX_3. The second region of interest in this spectrum is the region near 875 cm^{-1}. As already mentioned, the transition moment vector associated with this absorption is perpendicular to the plane of the benzene ring. As in the earlier studies[5,16], it was necessary to use two Lorentzian peaks to obain a good fit in that region. These two Lorentzian peaks are at 872 and 877 cm^{-1}.

Refractive index measurements

An Abbe refractometer equipped with a polarizer was used to measure the three principal refractive indices of the films.

PRIMARY DATA AND TESTS OF DIFFERENT CORRECTIONS

Raman scattered intensities

In *Table 1*, the Raman scattered intensities I_{ij} show clearly that the samples are biaxially oriented. I_{11} and I_{22} are not equal, nor are I_{13} and I_{23}. It should be noted that the ratios I_{11}/I_{22} and I_{13}/I_{23} are smaller than unity. This unexpected tendency has been found previously for the first biaxially oriented sample studied by Jarvis *et al.*[5], but not for the second range of biaxial films studied[9]. The two ratios I_{11}/I_{22} and I_{13}/I_{23} tend to increase with increasing stress at a given drawing temperature and, at the highest stress, nearly reach unity, the value expected for uniaxially oriented samples.

Comparison of molecular orientation calculated with and without the assumption of a uniaxial tensor for the 1616 cm^{-1} Raman line

It has been shown recently[6] that the Raman tensor for the 1614 cm^{-1} line of bis(2-hydroxyethyl)terephthalate, a model compound for PET, is not quite uniaxial. The principal axes of the tensor were shown, however, to be very close to $Ox_1^rx_2^rx_3^r$. When the principal axes were assumed to be parallel to the axes of that system, the following values of r_1 and r_2 were found:

$$r_1 = \alpha_1/\alpha_3 = -0.22 \quad \text{and} \quad r_2 = \alpha_2/\alpha_3 = -0.04$$

These two values must be very close to the real values for the 1616 cm^{-1} PET Raman line. It should be noted that α_1 and α_2 are actually very different.

Combining equations (2a) to (2f), (7a) and (7b), a system of eight linear equations in the 14 quantities $(\alpha_3^2 I_0 N_0)^{-1}$, P_{lmn}^r for $l = 2$ and $l = 4$ is obtained. This system cannot be solved without any assumptions. An iterative procedure has to be used. In this particular case, F, G and H are very small compared with A, B, C, D and E.

In the first step of the iteration, F, G and H are set equal to zero. As a consequence, the system of equations reduces to a system of eight independent linear equations

Table 1 Raman intensities I_{ij} ($1616\,cm^{-1}$): mean values (root mean square deviations)

T (°C)	σ_0 (MPa)	I_{11}	I_{22}	I_{33}	I_{12}	I_{13}	I_{23}
90	1.84	33.73	45.62	100.00	31.32	25.51	54.69
		(1.69)	(4.94)	(2.26)	(2.56)	(1.62)	(2.90)
90	3.07	20.58	26.13	100.00	20.03	22.17	28.93
		(0.82)	(1.05)	(0.52)	(0.83)	(1.23)	(1.36)
90	4.30	20.55	20.61	100.00	15.68	17.90	20.74
		(0.50)	(1.80)	(0.17)	(1.61)	(0.75)	(1.26)
90	5.52	19.77	19.81	100.00	14.67	17.41	20.42
		(1.06)	(1.14)	(0.47)	(1.07)	(0.42)	(1.47)
100	1.23	27.77	41.78	100.00	29.66	28.16	40.21
		(1.90)	(0.97)	(1.96)	(2.36)	(4.82)	(3.46)
100	2.46	20.09	23.33	100.00	19.34	19.27	24.62
		(1.34)	(1.24)	(0.44)	(1.23)	(1.59)	(1.39)
100	3.69	16.42	21.70	100.00	16.78	18.82	22.55
		(0.85)	(1.05)	(0.27)	(1.72)	(1.10)	(1.48)
100	4.92	14.44	17.72	100.00	14.67	17.99	21.85
		(1.01)	(0.66)	(0.44)	(1.60)	(1.49)	(1.59)

Table 2 Values of P^r_{lmn} calculated for two films drawn at 90°C

σ_0 (MPa)	Method[a]	P^r_{200}	P^r_{220}	P^r_{202}	P^r_{222}	P^r_{400}	P^r_{420}	P^r_{440}
1.84	a	0.183	−0.027	0.024	0.059	0.029	−0.012	−0.006
	b	0.185	−0.028	0.024	0.060	0.030	−0.013	−0.008
5.52	a	0.369	−0.003	0.043	0.065	0.203	−0.002	−0.005
	b	0.371	−0.003	0.041	0.065	0.193	−0.004	−0.005

[a] a: $r = r_1 = r_2 = -0.15$; b: $r_1 = -0.22$ and $r_2 = -0.04$

in the eight quantities $(\alpha_3^2 I_0 N_0)^{-1}$, P^r_{2mn}, P^r_{400}, P^r_{420}, P^r_{440}. Therefore these seven orientation moment averages P^r_{lmn} can be calculated. The 'most probable' distribution function $N^r_{mp}(\theta^r, \phi^r, \psi^r)$ to which they correspond can then be calculated and is given by[7]:

$$N^r_{mp}(\theta^r, \phi^r, \psi^r) = \exp\left[\sum_{lmn} A_{lmn} p_{lmn}(\theta^r, \phi^r, \psi^r)\right] \quad (10)$$

where the sum extends over all lmn for which P^r_{lmn} are known and the A_{lmn} must be chosen so that these values are given correctly. This 'most probable' distribution function allows the estimation of the six remaining P^r_{4mn}.

The second step of the iteration consists of using these six values, P^r_{402}, P^r_{404}, P^r_{422}, P^r_{424}, P^r_{442} and P^r_{444}, as constants in equations (2a) to (2f), (7a), (7b) with the real values of F, G and H. Then a new set of P^r_{2mn}, P^r_{400}, P^r_{420}, P^r_{440} can be determined, which leads to a new 'most probable' distribution function and then to the calculation of six new values for P^r_{402}, P^r_{404}, P^r_{422}, P^r_{424}, P^r_{442} and P^r_{444}.

This procedure can be followed n times and stopped when the 13 P^r_{lmn} do not change significantly at the last step of iteration.

Table 2 shows P^r_{2mn}, P^r_{400}, P^r_{420}, P^r_{440} calculated for two films drawn at 90°C with two different stresses ($\sigma_0 = 1.84$ and $5.52\,MPa$). Rows labelled 'a' were calculated using the method of Jarvis *et al.*[5], assuming a uniaxial Raman tensor and[5,6,9] $r = r_1 = r_2 = -0.15$. Rows labelled 'b' were calculated for $r_1 = -0.22$ and $r_2 = -0.04$ using the iterative procedure described above with $n = 2$ steps of iteration. The differences between the two sets of values are smaller than the uncertainty in the values arising from the uncertainty in the intensity measurements that can be estimated at 6%. This shows clearly that the most important properties of this Raman tensor, as far as orientation calculations are concerned, are that both α_1 and α_2 are very small compared to α_3 and that they are of the same sign, so that only one direction Ox^r_3 is characteristic for this tensor, and it can be considered as uniaxial.

As a consequence, only values calculated assuming a uniaxial Raman tensor for the $1616\,cm^{-1}$ line and $r = -0.15$ will be considered in the remaining discussion, and therefore the same calculation procedure was used to determine P^r_{200}, P^r_{220}, P^r_{400}, P^r_{420}, P^r_{440} from the Raman data and P^r_{202}, P^r_{222} from the infrared data as in earlier work[5].

Effect of optical anisotropy on Raman scattering

In the calculation of the relative Raman intensities, I_{ij}, all the effects due to the differences of refractive index for different directions of polarization were neglected, as in earlier work dealing with orientation in PET films[5,9]. Several corrections depending on the refractive indices should in fact be applied to these intensities. These corrections were first introduced by Nobbs *et al.*[25] and

were further developed by Lewis and Bower[6]. The three main corrections are due to the dependence of the transmission coefficients for the incident and scattered light on the polarization direction, the two Dexter[26] coefficients for the absorption and emission probability for an atom embedded in a medium of refractive index n ($\neq 1$), and the cone angle factor. Assuming a uniaxial Raman tensor, these corrections will affect only the orientation averages of Ox'_3 and not those of Ox'_2, since the latter are determined directly from the infrared measurements.

The relative intensities I_{ij} with $I_{33} = 100$, calculated by including the refractive index corrections, are shown in *Table 3* for the films stretched at 90°C. These intensities are fairly close to those calculated without taking this correction into account. It should also be noted that the general pattern of behaviour does not change. For example, I_{11} is still smaller than I_{22}, I_{23} greater than I_{13}, and I_{11}/I_{22} and I_{13}/I_{23} still increase with increasing stress.

In *Table 4*, P'_{200}, P'_{220}, P'_{400}, P'_{420}, P'_{440} calculated from the Raman data are given for two samples stretched at 90°C with $\sigma_0 = 1.84$ and 5.52 MPa. Rows labelled 'a' were calculated without the refractive index corrections and rows labelled 'b' were calculated with the corrections.

It is clear that the corrections do not significantly affect the final results. In view of this and the fact that their applicability[6] has not yet been completely established, they will be neglected in the remaining discussion.

Table 3 Raman intensities I_{ij} (1616 cm^{-1}) for four films drawn at 90°C calculated with the refractive index correction: mean values (root mean square deviations)

σ_0 (MPa)	I_{11}	I_{22}	I_{33}	I_{12}	I_{13}	I_{23}
1.84	36.31	50.19	100.00	34.15	26.49	57.39
	(1.84)	(5.27)	(2.44)	(2.75)	(1.73)	(3.04)
3.07	22.46	29.41	100.00	22.23	23.18	30.72
	(0.89)	(1.13)	(0.58)	(0.91)	(1.30)	(1.45)
4.30	23.13	24.24	100.00	17.63	19.03	22.52
	(0.57)	(1.99)	(0.20)	(1.78)	(0.88)	(1.47)
5.52	22.67	23.93	100.00	17.32	18.66	22.46
	(1.25)	(1.29)	(0.57)	(1.22)	(0.50)	(1.63)

OVERALL MOLECULAR ORIENTATION

Orientation averages

The seven orientation moment averages P'_{lmn} are given in *Table 5*. At a given temperature, P'_{200} increases with increasing applied stress, i.e. the C_7–C_8 axes of the benzene rings tend to orient more and more towards the draw direction OX_3. The most surprising result is that P'_{220} has a negative value for all films. That means that the C_7–C_8 axes of the benzene rings tend to lie out of, more than in, the plane of the film. This unusual result has already been found on a uniaxial-planar PET film studied by Jarvis *et al.*[5]. It should be noted that this tendency decreases with increasing stress at a given temperature as P'_{220} decreases. The distribution of Ox'_3 is nearly uniaxial towards the draw direction for high stresses as P'_{220} is very close to zero.

For a better understanding of the orientation of the three Ox'_i axes, the values of P'_{2mn} were used to calculate the averages $\langle \cos^2(x'_i OX_j) \rangle$ which are shown in *Table 6*. For all tables dealing with these averages, the results for one sample are displayed as follows:

$$\begin{bmatrix} x'_1OX_1 & x'_1OX_2 & x'_1OX_3 \\ x'_2OX_1 & x'_2OX_2 & x'_2OX_3 \\ x'_3OX_1 & x'_3OX_2 & x'_3OX_3 \end{bmatrix}$$

In *Table 6*, all the $\langle \cos^2(x'_3 OX_j) \rangle$ are dependent only on the Raman measurements and all the $\langle \cos^2(x'_2 OX_j) \rangle$ are dependent only on the infrared data. For randomly oriented benzene rings, all these averages would have a

Table 4 Values of P'_{lmn} calculated from the Raman and infrared data for two films drawn at 90°C

σ_0 (MPa)	Method[a]	P'_{200}	P'_{220}	P'_{202}	P'_{222}	P'_{400}	P'_{420}	P'_{440}
1.84	a	0.183	−0.027	0.024	0.059	0.029	−0.012	−0.006
	b	0.163	−0.028	0.028	0.060	0.027	−0.012	−0.006
5.52	a	0.369	−0.003	0.043	0.065	0.203	−0.002	−0.005
	b	0.324	−0.005	0.052	0.067	0.179	−0.002	−0.005

[a] a: Without any corrections; b: with the refractive index correction

Table 5 Values of P'_{lmn} calculated from the Raman and infrared data

T (°C)	σ_0 (MPa)	P'_{200}	P'_{220}	P'_{202}	P'_{222}	P'_{400}	P'_{420}	P'_{440}
90	1.84	0.183	−0.027	0.024	0.059	0.029	−0.012	−0.006
90	3.07	0.304	−0.011	0.025	0.048	0.099	−0.004	−0.007
90	4.30	0.358	−0.003	0.030	0.059	0.196	−0.002	−0.005
90	5.52	0.369	−0.003	0.043	0.065	0.203	−0.002	−0.005
100	1.23	0.204	−0.019	0.029	0.058	0.022	−0.005	−0.008
100	2.46	0.321	−0.009	0.035	0.077	0.157	−0.003	−0.008
100	3.69	0.350	−0.007	0.038	0.078	0.182	−0.002	−0.007
100	4.92	0.396	−0.007	0.041	0.092	0.182	−0.002	−0.007

Table 6 Values of $\langle\cos^2(x_i^r OX_j)\rangle$ for all the samples

	X_1	X_2	X_3
x_1^r	0.426	0.254	0.320
x_2^r	0.356	0.419	0.225
x_3^r	0.218	0.326	0.455

$T = 90°C$ $\sigma_0 = 1.84$ MPa

0.415	0.278	0.323
0.358	0.434	0.208
0.227	0.303	0.469

$T = 100°C$ $\sigma_0 = 1.23$ MPa

0.418	0.300	0.282
0.372	0.446	0.182
0.210	0.254	0.536

$T = 90°C$ $\sigma_0 = 3.07$ MPa

0.438	0.266	0.296
0.354	0.489	0.157
0.208	0.244	0.547

$T = 100°C$ $\sigma_0 = 2.46$ MPa

0.425	0.301	0.274
0.367	0.479	0.154
0.208	0.220	0.572

$T = 90°C$ $\sigma_0 = 4.30$ MPa

0.439	0.269	0.293
0.358	0.502	0.140
0.203	0.231	0.567

$T = 100°C$ $\sigma_0 = 3.69$ MPa

0.420	0.284	0.296
0.376	0.499	0.125
0.204	0.216	0.579

$T = 90°C$ $\sigma_0 = 5.52$ MPa

0.457	0.259	0.283
0.356	0.524	0.120
0.187	0.215	0.597

$T = 100°C$ $\sigma_0 = 4.92$ MPa

value of 1/3 and for a fully oriented sample with Ox_i^r parallel to the corresponding OX_i, the average value would be δ_{ij}. The data in *Table 6* indicate clearly an increasing tendency towards this type of orientation with increasing stress at a given drawing temperature.

As shown already by the study of P_{200}^r and P_{220}^r, the following conclusions can be drawn about the orientation of Ox_3^r from this table.

(1) $\langle\cos^2(x_3^r OX_3)\rangle$ increases with increasing stress, showing that the preferred orientation of the Ox_3^r is parallel to the draw direction and increases with stress.
(2) $\langle\cos^2(x_3^r OX_1)\rangle$ is slightly smaller than $\langle\cos^2(x_3^r OX_2)\rangle$. This indicates that Ox_3^r tends to lie more normal than parallel to the plane of the film, but this tendency seems to decrease with increasing stress, as the two values tend to become equal. As a consequence, the distribution of the Ox_3^r axes becomes more and more uniaxial with increasing stress.

The second interesting feature of *Table 6* concerns the orientation of the benzene ring normal Ox_2^r, given by $\langle\cos^2(x_2^r OX_j)\rangle$. For uniaxial symmetry, $\langle\cos^2(x_2^r OX_1)\rangle$ is equal to $\langle\cos^2(x_2^r OX_2)\rangle$, but in this study, $\langle\cos^2(x_2^r OX_2)\rangle$ is greater than $\langle\cos^2(x_2^r OX_1)\rangle$, which shows the tendency of the planes of the benzene rings to lie in the plane of the film. This tendency increases with increasing stress as the second average seems to remain constant and the first to increase. The same pattern of behaviour was found in the earlier study on the refractive indices[4].

Distribution functions and stereographic projections

In order to get a better feeling for the meaning of these averages, the 'most probable' distribution function for the benzene ring orientation, $N_{mp}^r(\theta^r, \phi^r, \psi^r)$, as defined earlier in this paper, has been calculated from the seven known P_{lmn}^r. A computer program has been used to calculate the A_{lmn}. The form of graphical representation chosen for this 'most probable' distribution function was to display, for each sample, the stereographic projection of the distribution of orientations of the Ox_3^r axes in the OX_1X_2 plane (integration being performed over all values of ψ^r for a given value of θ^r and ϕ^r) and the stereographic projection of the distribution of orientations of the Ox_r^2 axes in the OX_1X_3 plane (integration being performed over all values of $\psi^{r'}$ for a given value of $\theta^{r'}$ and $\phi^{r'}$, where $\theta^{r'}$, $\phi^{r'}$ and $\psi^{r'}$ are the Euler angles with respect to axes $OX_1'X_2'X_3'$ with $OX_1' = OX_3$, $OX_2' = OX_1$ and $OX_3' = OX_2$. The contours on these stereographic projections are at equal intervals in the value of the distribution function between zero and its highest value.

The stereographic projections of the distribution of orientation of Ox_3^r in the OX_1X_2 plane and of the Ox_2^r axes in the OX_1X_3 plane are given for all films in *Figure 2*. It can be seen that, at low stresses and for the two drawing temperatures considered, the Ox_3^r axes are more oriented out of the plane of the film than in the plane. At 90°C, for the lowest stress, the central peak is divided into two peaks that are out of the plane of the film. However, with increasing stress the contours of the distribution of Ox_3^r become more and more circular, indicating a fairly uniaxial distribution. The existence of the double peak for the sample drawn under the lowest stress at 90°C is linked with the high (negative) value of P_{420}^r found for this sample (see *Table 5*). The data for the other samples would suggest a value of about -0.006, where the observed value is twice as large. Reducing P_{420}^r to -0.006 removes the double peak, but the required change is very large compared to the estimated uncertainty of ± 0.002. It thus seems likely that the double peak is real.

As far as the distribution of the Ox_2^r axes is concerned, the tendency of this axis to orient along the normal to the film is clearly seen. For small stresses, the distribution has two maxima in the OX_1X_2 plane but tends to have only one central peak for high stresses. The double peak is not removed by changing P_{420}^r to -0.006 for the sample discussed above.

AMORPHOUS AND CRYSTALLINE CONTRIBUTIONS

Crystalline orientation averages

In earlier work[3] on these samples, as a result of the experimental procedure used, only the second moment averages for the orientation distribution of the $(\bar{1}05)$ and (100) plane normals were calculated from the X-ray data. Assuming the crystalline unit cell described by Daubeny *et al.*[19], the second-moment averages of the orientation distribution for the benzene ring axes in the crystalline phase, P_{2mn}^r(crystals), can be calculated as well as the second-moment averages of the c-axis distribution for the crystallites with respect to the draw direction, P_{2m0}(c-axis). The values of P_{200}(c-axis) range from 0.95 to 0.985, from which it can be concluded that the chain axes in the crystalline phase, which are parallel to the c-axis, are strongly oriented toward the draw direction.

The values of $\langle\cos^2(x_i^r OX_j)\rangle$(crystals) were calculated from the P_{2mn}^r(crystals) and are given in *Table 7*. It should be noted that, in the unit cell described by Daubeny *et al.*[19], the angle between the c-axis and the C_7–C_8 axis is 21.7°, so that the maximum achievable value for $\langle\cos^2(x_3^r OX_3)\rangle$(crystals) with the c-axis fully oriented along the draw direction is 0.863. *Table 7* shows the following facts.

(1) The values of $\langle\cos^2(x_3^r OX_3)\rangle$(crystals) remains

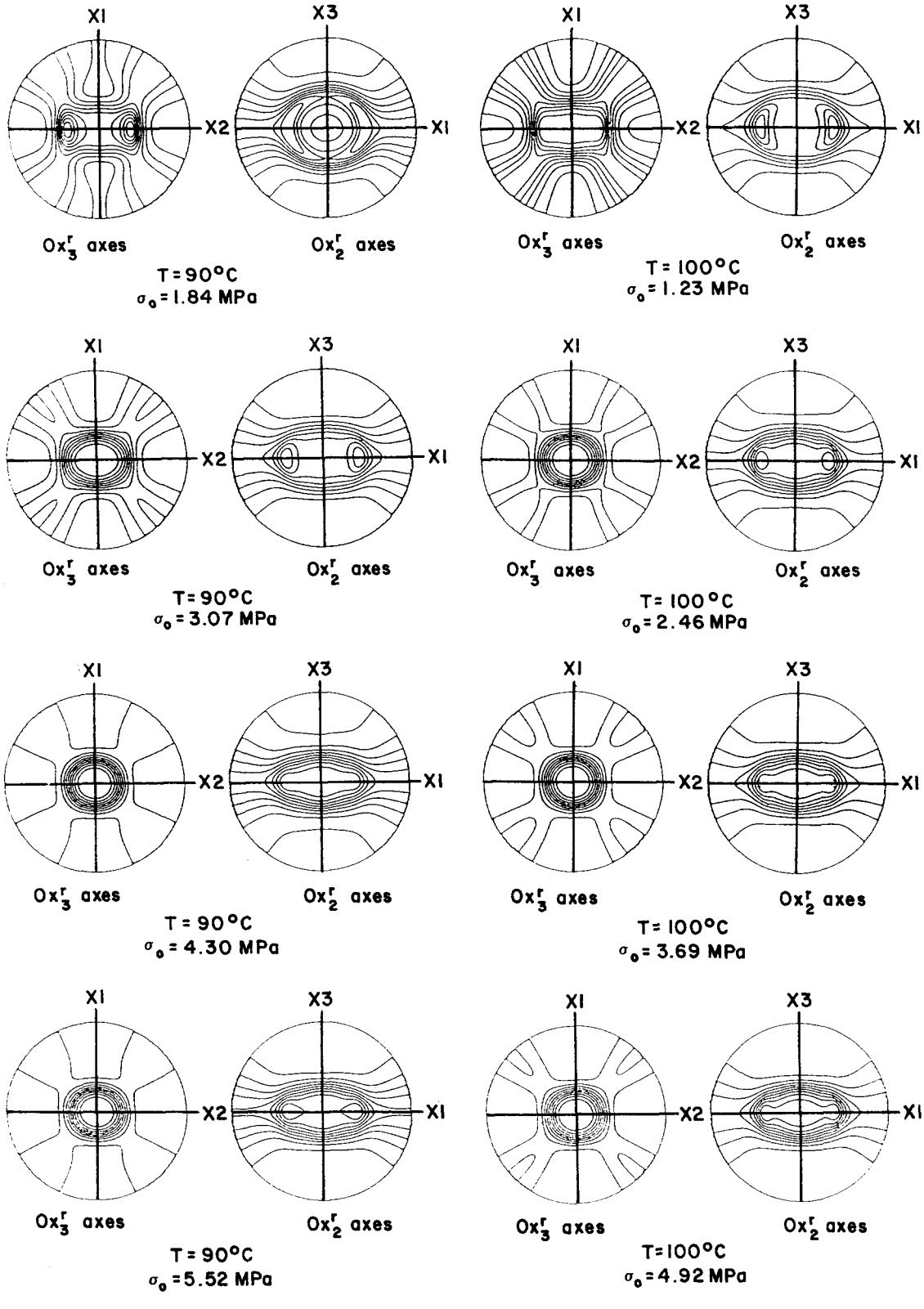

Figure 2 Stereographic projections of the 'most probable' distribution function of the benzene ring orientation for all the samples, calculated from the seven known P^r_{lmn}. Note that the distribution of Ox'_3 in the regions for high values of θ and $\phi = \pi/4 + n\pi/2$ shows a small maximum, not a minimum

fairly constant with stress and temperature. This corresponds to the fact that the chain axis is nearly fully oriented along the draw direction and therefore this average is near its maximum value.

(2) The value of $\langle \cos^2(x'_3OX_1)\rangle$(crystals) is bigger than that of $\langle \cos^2(x'_3OX_2)\rangle$(crystals), which indicates that in the crystalline phase the C_7–C_8 axes tend to lie in rather than out of the plane of the film.

(3)The difference between $\langle \cos^2(x'_2OX_2)\rangle$(crystals) and $\langle \cos^2(x'_2OX_1)\rangle$(crystals) is very large and increases with increasing stress. The planes of the benzene rings tend to orient more and more in the plane of the film.

Table 7 Values of $\langle \cos^2(x_i^r OX_j) \rangle$(crystals)

$\begin{bmatrix} 0.554 & 0.324 & 0.122 \\ 0.336 & 0.622 & 0.042 \\ 0.110 & 0.054 & 0.836 \end{bmatrix}$	$\begin{bmatrix} 0.586 & 0.300 & 0.114 \\ 0.304 & 0.654 & 0.042 \\ 0.110 & 0.046 & 0.844 \end{bmatrix}$
$T = 90°C$ $\sigma_0 = 1.84$ MPa	$T = 100°C$ $\sigma_0 = 1.23$ MPa
$\begin{bmatrix} 0.614 & 0.262 & 0.124 \\ 0.270 & 0.694 & 0.036 \\ 0.116 & 0.044 & 0.840 \end{bmatrix}$	$\begin{bmatrix} 0.656 & 0.224 & 0.124 \\ 0.228 & 0.740 & 0.032 \\ 0.116 & 0.036 & 0.848 \end{bmatrix}$
$T = 90°C$ $\sigma_0 = 3.07$ MPa	$T = 100°C$ $\sigma_0 = 2.46$ MPa
$\begin{bmatrix} 0.628 & 0.250 & 0.122 \\ 0.258 & 0.713 & 0.029 \\ 0.114 & 0.038 & 0.846 \end{bmatrix}$	$\begin{bmatrix} 0.668 & 0.212 & 0.121 \\ 0.215 & 0.757 & 0.028 \\ 0.117 & 0.033 & 0.857 \end{bmatrix}$
$T = 90°C$ $\sigma_0 = 4.30$ MPa	$T = 100°C$ $\sigma_0 = 3.69$ MPa
$\begin{bmatrix} 0.651 & 0.229 & 0.120 \\ 0.235 & 0.736 & 0.029 \\ 0.114 & 0.034 & 0.851 \end{bmatrix}$	$\begin{bmatrix} 0.678 & 0.201 & 0.121 \\ 0.205 & 0.772 & 0.025 \\ 0.119 & 0.027 & 0.854 \end{bmatrix}$
$T = 90°C$ $\sigma_0 = 5.52$ MPa	$T = 100°C$ $\sigma_0 = 4.92$ MPa

Amorphous orientation

Assuming a two-phase model, it can easily be shown that:

$$P^r_{2mn}(\text{amorphous}) = \frac{1}{1-\chi_c}[P^r_{2mn} - \chi_c P^r_{2mn}(\text{crystals})] \tag{11}$$

The calculated orientation moment averages of the distribution of the benzene rings in the amorphous phase thus depend on the crystallinity. As pointed out earlier, the crystallinity used in this study is determined from the density, assuming a two-phase model. As a consequence, the calculated value of the crystallinity depends on the crystalline density d_c. The results presented in this work were calculated with $d_c = 1.455$ (which is the most commonly used value of d_c). The calculations were also carried out with the maximum published value of the crystalline density $d_c = 1.484$ and no changes appear in the general behaviour of the results for the amorphous phase.

As for the other sets of P^r_{2mn}, the P^r_{2mn}(amorphous) have been transformed into $\langle \cos^2(x_i^r OX_j) \rangle$(amorphous). As an example, the nine $\langle \cos^2(x_i^r OX_j) \rangle$(amorphous) determined from the second-order moment averages of the orientation distribution for the benzene rings in the amorphous phase, calculated with both extreme values of d_c, are given in *Table 8* for a film stretched with $T = 90°C$ and $\sigma_0 = 4.30$ MPa.

In *Table 9*, the $\langle \cos^2(x_i^r OX_j) \rangle$(amorphous) are given for all the samples. The table shows the following features.

(1) For the amorphous phase, the C_7–C_8 axis orientation with respect to the draw direction OX_3 increases with increasing stress, as shown by $\langle \cos^2(x_3^r OX_3) \rangle$(amorphous). This axis tends to be more out of than in the plane of the film. This latter behaviour is strong for small stresses but decreases with increasing stress.

(2) The behaviour of Ox_2^r, the benzene ring normal, in the amorphous phase is very interesting. The very strong tendency of this axis to orient along the normal to the plane of the film, OX_2, as observed in the crystalline phase, appears to be very weak in the amorphous phase and is almost negligible for $T = 100°C$, as $\langle \cos^2(x_2^r OX_2) \rangle$(amorphous) and $\langle \cos^2(x_2^r OX_1) \rangle$(amorphous) are very similar. No characteristic variations of the difference between those two values at a given temperature can be seen as a function of stress. The same pattern of behaviour of the benzene ring normals in the amorphous phase was also found by combining X-ray and refractive index measurements[4].

The essentially uniaxial nature of the orientation of both the C_1–C_4 and benzene ring normal directions does not, however, mean that the orientation of the normal to the ring plane is uniaxial around the C_1–C_4 axis. If this were so, i.e. if ψ^r were independent of ϕ^r, then

$$P^n_{200}(\text{amorphous}) = \langle \tfrac{1}{2}(3\cos^2(x_2^r OX_3)(\text{amorphous}) - 1) \rangle$$

would be equal to $-0.5P^r_{200}$(amorphous) where P^n_{200} refers to the ring normal. The data in *Table 9* show that this is not the case. It is easy to show that the maximum value of P^n_{200} is given by $\frac{1}{2} - P^r_{200}$, which is found if all ring normals lie in the plane containing the C_1–C_4 axis and the draw direction, and that its minimum value is $-\frac{1}{2}$, if all ring normals are perpendicular to this plane. *Figure 3* shows that for all samples and for both crystalline and amorphous material the actual distribution is somewhere between the latter extreme and that for ψ^r independent of ϕ^r. The benzene rings tend to turn their smallest cross-section in the direction of stretching. A similar tendency has already been found for solute

Table 8 Values of $\langle \cos^2(x_i^r OX_j) \rangle$(amorphous) for a sample drawn at $T = 90°C$ and $\sigma_0 = 4.30$ MPa

$\begin{bmatrix} 0.384 & 0.312 & 0.305 \\ 0.388 & 0.432 & 0.181 \\ 0.229 & 0.257 & 0.515 \end{bmatrix}$	$\begin{bmatrix} 0.393 & 0.309 & 0.298 \\ 0.383 & 0.443 & 0.174 \\ 0.222 & 0.250 & 0.528 \end{bmatrix}$
$d_c = 1.455$	$d_c = 1.484$

Table 9 Values of $\langle \cos^2(x_i^r OX_j) \rangle$(amorphous)

$\begin{bmatrix} 0.412 & 0.246 & 0.342 \\ 0.358 & 0.396 & 0.246 \\ 0.230 & 0.358 & 0.411 \end{bmatrix}$	$\begin{bmatrix} 0.374 & 0.252 & 0.374 \\ 0.370 & 0.384 & 0.246 \\ 0.256 & 0.364 & 0.381 \end{bmatrix}$
$T = 90°C$ $\sigma_0 = 1.84$ MPa	$T = 100°C$ $\sigma_0 = 1.23$ MPa
$\begin{bmatrix} 0.393 & 0.305 & 0.302 \\ 0.385 & 0.413 & 0.202 \\ 0.222 & 0.282 & 0.497 \end{bmatrix}$	$\begin{bmatrix} 0.372 & 0.278 & 0.350 \\ 0.392 & 0.414 & 0.194 \\ 0.236 & 0.308 & 0.457 \end{bmatrix}$
$T = 90°C$ $\sigma_0 = 3.07$ MPa	$T = 100°C$ $\sigma_0 = 2.46$ MPa
$\begin{bmatrix} 0.384 & 0.312 & 0.305 \\ 0.388 & 0.432 & 0.181 \\ 0.229 & 0.257 & 0.515 \end{bmatrix}$	$\begin{bmatrix} 0.367 & 0.286 & 0.347 \\ 0.403 & 0.421 & 0.175 \\ 0.229 & 0.293 & 0.478 \end{bmatrix}$
$T = 90°C$ $\sigma_0 = 4.30$ MPa	$T = 100°C$ $\sigma_0 = 3.69$ MPa
$\begin{bmatrix} 0.363 & 0.297 & 0.340 \\ 0.411 & 0.441 & 0.148 \\ 0.226 & 0.262 & 0.512 \end{bmatrix}$	$\begin{bmatrix} 0.380 & 0.280 & 0.340 \\ 0.408 & 0.440 & 0.152 \\ 0.212 & 0.280 & 0.509 \end{bmatrix}$
$T = 90°C$ $\sigma_0 = 5.52$ MPa	$T = 100°C$ $\sigma_0 = 4.92$ MPa

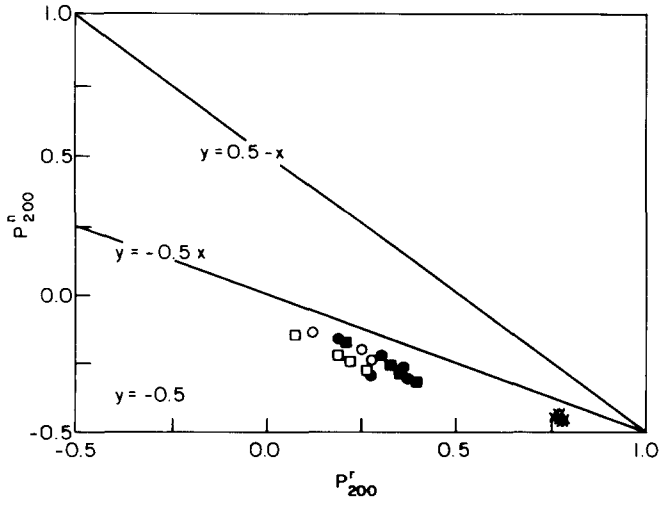

Figure 3 Orientation moment average P^n_{200} of the normals to the benzene ring with respect to the draw direction *versus* P^r_{200}: for the overall sample with $T = 90°C$ (●) and $T = 100°C$ (■); in the amorphous phase with $T = 90°C$ (○) and $T = 100°C$ (△); in the crystalline phase with $T = 90°C$ (+) and $T = 100°C$ (×)

aromatic molecules within uniaxially stretched polyethylene as solvent[27,28].

Stereographic projections of the amorphous and crystalline orientation

As far as the amorphous and the crystalline phases are concerned, only the second moment averages of the orientation distribution of the benzene rings are known. In this part of the study, the 'most probable' distribution function for each phase, and also for the overall sample, have therefore been calculated from the simplest form of equation (10) in which only the four second-order orientation moment averages are used to determine the four A_{2mn}.

The stereographic projections of the benzene ring orientation distributions for the overall sample, and for the amorphous and crystalline phases are given in *Figure 4* for two films drawn at 100°C with $\sigma_0 = 1.23$ and

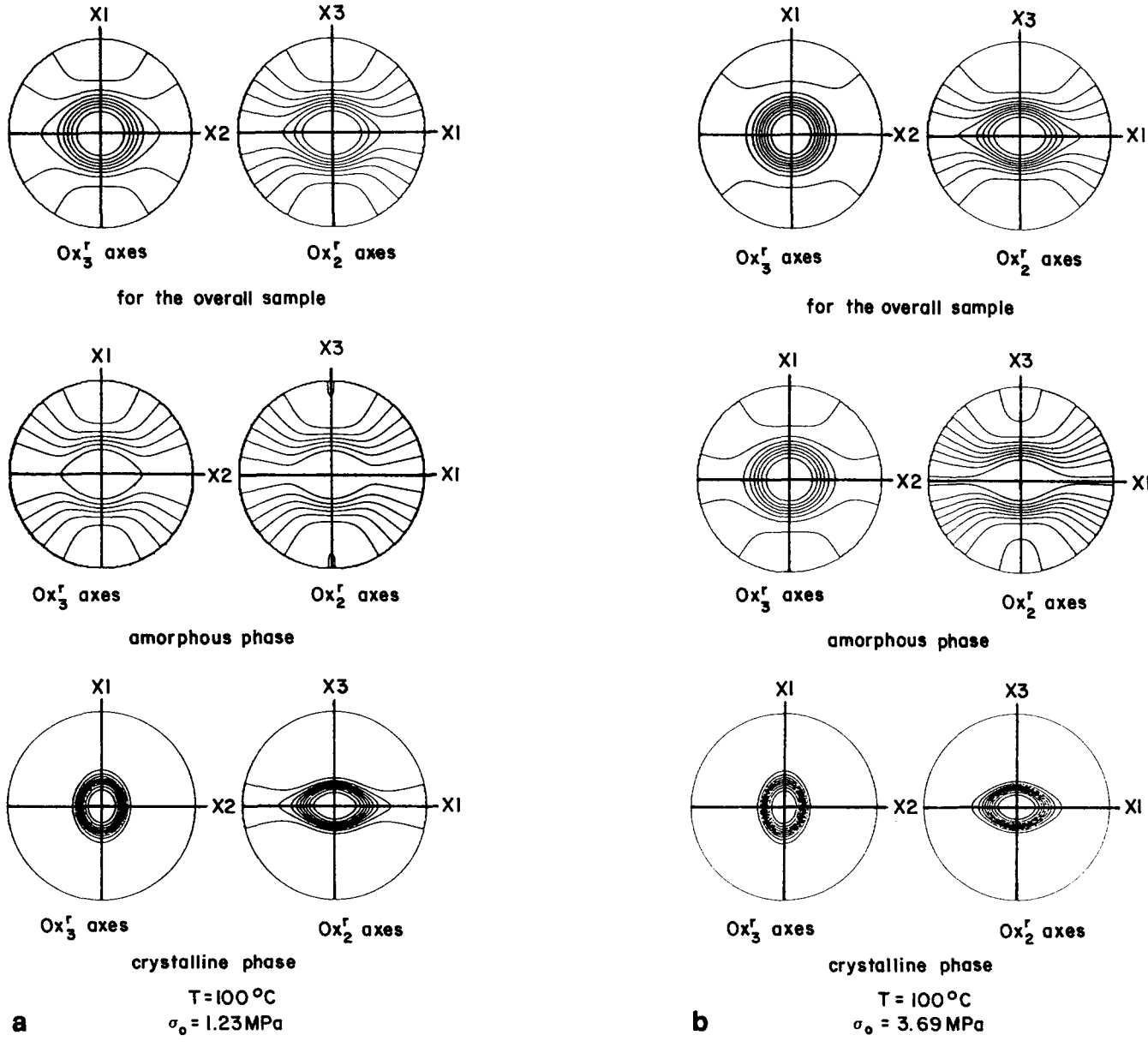

Figure 4 Stereographic projections of the 'most probable' distribution function of the benzene ring orientation calculated from the second moment orientation averages: crystalline and amorphous contributions: (a) $T = 100°C$, $\sigma_0 = 1.23$ MPa; (b) $T = 100°C$, $\sigma_0 = 3.69$ MPa

3.69 MPa. All the differences between the distribution of orientations of the benzene rings and its evolution with stress in the amorphous phase compared to those of the crystalline phase, described above, appear very clearly on these projections.

CONCLUSION

Raman scattering and infrared absorption measurements have been used to determine moment averages of the benzene ring orientation distribution function for samples of films stretched under constant load, at constant width and in the region of the glass transition. The amorphous and crystalline contributions were obtained by combining these results with wide-angle X-ray diffraction measurements.

The assumption of a uniaxial tensor for the 1616 cm^{-1} Raman line has been proved to be a good approximation for the calculation of orientation moment averages for biaxial as well as uniaxial samples.

The use of refractive index corrections on Raman intensities does not change the results qualitatively and only changes them quantitatively by a small amount.

For all the samples, the orientation of the C_7–C_8 axes with respect to the draw direction increases with drawing load: the orientation is always more out of the plane of the film than towards it, but this unusual tendency decreases with increasing load and the distribution of these axes becomes nearly uniaxial for high loads. This distribution is the average of the two distributions in the amorphous and crystalline phases. In the amorphous phase, the same general tendency is found, but in the crystalline phase, the C_7–C_8 axes tend to be more in the plane of the film. Since the c-axes of the crystallites are fairly fully oriented along the draw direction, the orientation of the C_7–C_8 axes with respect to this direction does not change with load.

For all the samples, the benzene ring normals tend to be parallel to the normal to the plane of the film and this tendency increases with increasing load. In the crystalline phase, this axis is highly oriented with respect to the normal to the plane of the film. In the amorphous phase the benzene ring normals do not have any strong preferred orientation in the plane perpendicular to the draw direction, but they do have a preferred orientation around the C_1–C_4 axes.

ACKNOWLEDGEMENT

We gratefully acknowledge Rhône-Poulenc for providing financial support to one of us (P.L.).

REFERENCES

1 Le Bourvellec, G., Beautemps, J. and Jarry, J. P. *J. Appl. Polym. Sci.* 1990, **39**, 319
2 Le Bourvellec, G. and Beautemps, J. *J. Appl. Polym. Sci.* 1990, **39**, 329
3 Lapersonne, P., Tassin, J. F., Monnerie, L. and Beautemps, J. *Polymer* 1991, **32**, 3331
4 Lapersonne, P., Tassin, J. F. and Monnerie, L. to be published
5 Jarvis, D. A., Hutchinson, I. J., Bower, D. I. and Ward, I. M. *Polymer* 1980, **21**, 41
6 Lewis, E. L. V. and Bower, D. I. *J. Raman Spectrosc.* 1987, **18**, 287
7 Bower, D. I. *Polymer* 1982, **23**, 1251
8 Lapersonne, P., Bower, D. I. and Ward, I. M. *Polymer* 1992, **33**, 1277
9 Bower, D. I., Jarvis, D. A. and Ward, I. M. *J. Polym. Sci., Polym. Phys. Edn.* 1986, **24**, 1459
10 Purvis, J., Bower, D. I. and Ward, I. M. *Polymer* 1973, **14**, 398
11 Purvis, J. and Bower, D. I. *J. Polym. Sci., Polym. Phys. Edn.* 1976, **14**, 1461
12 Bower, D. I., Jarvis, D. A., Lewis, E. L. V. and Ward, I. M. *J. Polym. Sci., Polym. Phys. Edn.* 1986, **24**, 1481
13 Bower, D. I. *J. Polym. Sci., Polym. Phys. Edn.* 1972, **10**, 2135
14 Bower, D. I. *J. Phys. (B)* 1976, **9**, 3275
15 Cunningham, A., Davies, G. R. and Ward, I. M. *Polymer* 1974, **15**, 743
16 Cunningham, A., Ward, I. M., Willis, H. A. and Zichy, V. *Polymer* 1974, **15**, 749
17 Hutchinson, I. J., Ward, I. M., Willis, H. A. and Zichy, V. *Polymer* 1980, **21**, 55
18 De Vries, A. J., Bonnebat, C. and Beautemps, J. *J. Polym. Sci., Polym. Phys. Edn.* 1977, **58**, 109
19 Daubeny, R., Bunn, C. W. and Brown, C. J. *Proc. R. Soc. (London)* 1954, **226**, 531
20 Astbury, W. T. and Brown, C. J. *Nature* 1946, **158**, 871
21 Fakirov, S., Fischer, E. W. and Schmidt, G. F. *Makromol. Chem.* 1975, **176**, 2459
22 Northolt, M. G. and Stuut, H. A. *J. Polym. Sci., Polym. Phys. Edn.* 1978, **16**, 939
23 Huisman, H. and Heuvel, H. M. *J. Appl. Polym. Sci.* 1978, **22**, 943
24 Purvis, J. and Bower, D. I. *Polymer* 1974, **15**, 645
25 Nobbs, J. H., Bower, D. I., Ward, I. M. and Patterson, D. *Polymer* 1974, **15**, 287
26 Dexter, D. L. in 'Solid State Physics', Vol. 6 (Eds F. Seitz and D. Turnbull), Academic Press, New York, 1958, p. 353
27 Radziszewski, J. G. and Michl, J. *J. Am. Chem. Soc.* 1986, **108**, 3291
28 Thulstrup, E. W. and Michl, J. *J. Am. Chem. Soc.* 1982, **104**, 5594